Accepted Manuscript

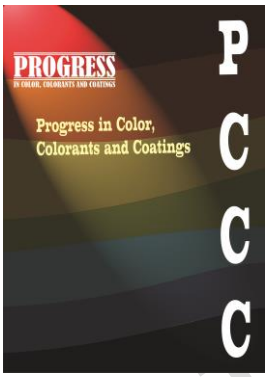

Title: Optimization of Color Stability in Graphene-based Hybrid Epoxy Coatings for Aerospace Applications Utilizing the Box–Behnken Design

Authors: Fatma İrem ŞAHİN, Yiğitalp OKUMUŞ, Nil ACARALI

Manuscript number**: PCCC-2602-1496**

To appear in: Progresss in Color, Colorants and Coatings

Received: 6 February 2026

Final Revised: 4 May 2026

Accepted: 6 May 2026

Please cite this article as:

F. İrem Şahin, Y. Okumus, Nil Aaarali, Optimization of Color Stability in Graphene-based Hybrid Epoxy Coatings for Aerospace Applications Utilizing the Box–Behnken Design, Prog. Color, Colorants, Coat., 20 (2027) XX-XXX.

DOI: 10.30509/pccc.2026.167770.1496

Optimization of Color Stability in Graphene-based Hybrid Epoxy Coatings for Aerospace Applications Utilizing the Box–Behnken Design

F. İrem Şahin [1], Y. Okumus [2], Nil Aaarali [1*]

[1] Department of Chemical Engineering, Yildiz Technical University, P.O. Box: 34220, Istanbul, Türkiye.

[2] TUSAŞ-Türk Havacılık ve Uzay Sanayii, P.O. Box: 06980, Ankara, Türkiye.

Emai: nbaran@yildiz.edu.tr, nilbaran@gmail.com

ABSTRACT

The present study aimed to investigate the surface color properties of graphene-based hybrid epoxy coatings using the CIE L*ab* color space (L*, a*, b*), total color difference, and chromaticity coordinates, with multivariate optimization performed through a Box–Behnken experimental design. Within the four-factor, three-level design space, L values ranged from 17.09 to 71.55, a* values from -2.18 to +0.27, b* values from 0.65 to 2.96, and ΔE values from 2.39 to 47.13. The minimum color difference (ΔE = 2.39) was obtained for the formulation containing 0.5 wt.% graphene, 0 wt.% boron carbide, 1 wt.% zinc borate, and 1 wt.% organic fiber, relative to black reference coating used in military aircraft. Response surface models showed high predictive capability, with R^2 values of 0.9920, 0.9912, 0.9922, and 0.9492 for L*, a*, b*, and ΔE, respectively. Analysis of variance showed that graphene content was the most influential factor affecting all color responses, particularly ΔE, due to its strong light-absorbing effect, which reduced surface lightness and suppressed color difference. The chromaticity coordinates of the coatings

were clustered within a narrow region of the diagram (x = 0.31-0.32, y = 0.33-0.34), while the correlated color temperature values were mainly in the range of 4550-5076 K. Overall, the results demonstrated that formulation control and ΔE minimization effectively improved color stability and camouflage compatibility in aerospace and defence coating applications, ensuring strong optical consistency.

Keywords: Color Space, CIE L*a*b, ΔE, Epoxy, Graphene

1. Introduction

Coating systems utilized in the aerospace and defence industries are designed to simultaneously provide properties such as corrosion resistance and environmental durability. The performance of coating systems and varnishes used in aircraft applications has been evaluated in terms of optical stability under long-term environmental exposure, as well as their mechanical and chemical properties [1, 2]. Since aerospace structures are multi-material, high-performance systems, protective coatings serve as barrier layers within primer, intermediate, and topcoat structures. Visser et al. emphasized that the aerospace sector has relied on hexavalent chromate-based systems for many years, but the development of chromate-free alternatives due to their toxicity has become a significant area of transformation for the sector [3]. The performance of aerospace coatings was also monitored through optical changes associated with atmospheric conditions. Changes in color coordinates were considered practical monitoring metrics that progressed together with the chemical and morphological degradation of the coating in accelerated aging tests [4]. In epoxy systems, performance was strongly dependent on

resin and hardener selection, as well as on the simultaneous optimization of these components [5, 6]. Experimental design-based studies have revealed that mixture components and formulation variables offer a suitable way to model coating properties and optimize them according to the targeted performance [7, 8]. One of the most widely used approaches for quantitatively evaluating color change in coatings is the CIE L*a*b (L*, a*, b*) color space, which shows a high correlation with human visual perception. In this system, L* represents the lightness–darkness of the surface, a* its position on the red–green axis, and b* its position on the yellow–blue axis. The total color difference (ΔE) derived from the space allows the comparison of different formulations and aging conditions by expressing the perceived color change of the surface as a single scalar parameter. In particular, the CIE 1976 ΔE definition has been widely used in the coatings and paints literature due to its simplicity and practical applicability [9, 10]. Studies have emphasized the use of optical metrics such as the color space and total color difference (ΔE) in conjunction with chemical and morphological analyses [11, 12]. Epoxy-based coatings have been widely used in both aerospace and industrial applications due to their strong adhesion, chemical resistance, and customizable formulations. However, the limited resistance of epoxy systems to UV radiation leads to optical problems such as binder degradation, yellowing, and surface dulling. Therefore, monitoring color changes in epoxy coatings through color parameters has emerged as a significant approach for evaluating coating performance [13, 14]. However, most studies on epoxy-based coatings have been conducted using single formulations. The relative and interactive effects of additive components on color coordinates in multifactorial systems have been addressed only to a limited extent [15, 16]. In addition, the direct optimization of color difference

with respect to a target reference coating color has remained quite limited in the literature [17]. It has been reported that filler and additive phases also significantly affect color parameters and color stability in polymer coatings. These findings strengthen the rationale for addressing color optimization using statistical approaches, as the additive ratios in the formulation can control the optical response (L*, a*, and b*-based color behavior) [18]. Virág et al. modelled the color change caused by thermal degradation as a function of temperature and TiO_2 content. They also reported that increasing the pigment content above a certain threshold no longer improved color retention. Such studies support the idea that, in coating design, adaptation to the target color, ΔE minimization, and the optimum range of additive levels can be determined by statistical models [19, 20]. Andrés-Herguedas et al. monitored the color change of alkyd- and acrylic-based coatings applied to concrete. They reported that, in some systems, acrylic-based coatings developed more pronounced color differences, while the green alkyd coating remained more resistant [21]. Chee et al. investigated bamboo/kenaf reinforced epoxy hybrid composites under accelerated aging conditions. Colorimetric analyses showed that the total color change became more pronounced, especially as the bamboo ratio increased. The study showed that environmental exposure also had detrimental effects on thermal stability, oxidative stability, and dynamic mechanical behavior, and that a 50:50 bamboo:kenaf ratio offered a more balanced combination of environmental resistance and degradability [22]. Ma et al. found that the increase in color number measured by colorimetry in oxidized aviation oils was related to oxidation products at the molecular level, and that this color change progressed together with important quality indicators such as acid number and tribological performance. This approach demonstrated that

visual and optical metrics could serve as a fast and practical monitoring tool in aviation applications [23]. LeVesque et al. developed transparent, colored, and black anodized coatings for passive thermal control applications on the International Space Station (ISS). The study aimed to improve the understanding of the optical properties of the coatings by controlling the anodization parameters. The study examined the balance between low reflectivity and high thermal performance desired in coating selection, especially for black coatings used in aerospace applications [24]. Graphene-based coating strategies have been evaluated as an effective barrier approach for maintaining the optical appearance and color stability of surfaces. Asadipour et al. reported that a transparent multilayer graphene coating on copper surfaces significantly reduced color change (ΔE) by suppressing oxidation at low temperatures. ΔE remained low in graphene-coated copper after oxidation, whereas a significant color deviation occurred in bare copper within a very short time [25].

This study focused on the development of hybrid water-based epoxy coatings containing graphene, boron carbide, zinc borate, and peanut shell-derived organic fiber, and evaluated their color performance through a statistical design approach. A Box–Behnken experimental design was employed to analyse the main, interaction, and quadratic effects of the formulation variables. The coatings were characterized mainly in terms of optical behavior using the L*, a*, b*, and ΔE, and their chromaticity coordinates were additionally assessed in the CIE 1931 color space. The statistical adequacy of the developed models was examined by ANOVA, while optical microscopy was used to compare the surface morphology of the optimized coatings. By combining formulation

design, color analysis, and model-based optimization, the study provides a practical framework for improving color matching effectiveness in epoxy-based camouflage coatings.

2. Experimental

2.1. Materials

In this study, water-based epoxy resin was used as the binder system. Graphene, boron carbide, zinc borate, and organic fiber were preferred as additive phases in the coating formulations. Graphene was included in the system due to its high light absorption capacity and opacifying effect; boron carbide for its role in regulating hardness and surface microstructure; zinc borate for its white pigment character and potential reflective effect; and organic fiber as an additive to increase light scattering and provide homogeneity on the surface. Organic fibers were obtained from peanut shells. Peanut shells collected from a local market in Istanbul were cleaned, sun-dried for three days, milled, and sieved to 90 μm. All chemicals were of analytical grade and supplied by Merck. For alkali treatment, 25 g of powder was treated with 0.5 M NaOH (750 mL) at 95°C for 2 h under constant stirring, then filtered, rinsed to neutral pH, and dried at 60°C. The resulting material was subsequently bleached with NaOCl after repeated washing until neutrality to obtain microcrystalline cellulose. Acid hydrolysis was then carried out by treating 5 g of MCC with 64 wt% H_2SO_4 (45 mL) at 50°C for 120 min. The reaction was stopped with cold water, followed by repeated washing to neutral pH and drying.

2.2. Methods

2.2.1. Experimental Design

A Box–Behnken experimental design was used to systematically investigate the effects of coating formulations on optical properties. Four independent variables were defined in the experimental design: (A) graphene ratio, (B) boron carbide ratio, (C) zinc borate ratio, and (D) organic fiber ratio. Each factor was considered at three levels (low, medium, and high), and the experimental matrix was constructed accordingly. The Box–Behnken design was preferred because it allowed for the modelling of interactions and second-order effects while keeping the number of experiments limited [26-28]. In this study, color differences (ΔE) were calculated in the CIE L*a*b* color space using the CIE 1976 formulation. ΔE values referred to the color difference between the coated samples and the target military camouflage reference coating and were denoted as ΔE. The target camouflage reference color was defined based on the literature reported color coordinates of a military black coating (BW400–9021), corresponding to the lowest thermal exposure condition reported by Michalski et al. [29]. To evaluate color stability after storage, the color difference between the initial measurement and the one-year stored condition was additionally calculated and denoted as ΔE_{store}. This parameter represented color drift over time and was independent of the reference color.

2.2.2. Coating Preparation

Coating formulations were prepared primarily by homogenizing the epoxy resin under mechanical mixing. Graphene, boron carbide, zinc borate, and organic fiber additives were gradually added to the resin in specified proportions, and controlled mixing was applied to prevent agglomeration. The resulting mixtures were applied to prepared

substrates. After curing, all samples were conditioned under standard ambient conditions prior to optical measurements.

2.2.3. Color Measurements

Color measurements of the coatings were performed using the L*, a*, b* color space. Measurements were taken from multiple points for each sample, and average values were calculated. The L* value represented the lightness-darkness of the surface, a* represented its position on the red-green axis, and b* represented its color component on the yellow-blue axis [30]. Total color difference (ΔE) was calculated according to the CIE 1976 definition using the measured L*, a*, and b* values.

2.2.4. Statistical Analysis and Optimization

Statistical analysis and modelling of experimental data were performed using Design-Expert software. Quadratic regression models were formed for L*, a*, b*, and ΔE responses. The suitability of the models was evaluated using analysis of variance (ANOVA). Statistical significance of factors and factor interactions was determined using p-values [31, 32]. Within the scope of optimization studies, the goal was to minimize the ΔE value; conversely, the aim was to keep the L*, a*, and b* coordinates as close as possible to the military reference color.

2.3. Characterization

2.3.1. Color Analysis

A colorimeter device (3nh NR100) was used for color measurements. The CIE L*a*b color

parameters (L*, a*, b*) were used in the device, where L* represented brightness and ranged between 0 (black) and 100 (white), a* represented the green (−) to red (+) axis, and b* represented the blue (−) to yellow (+) axis. Total color changes were calculated according to Eq. 1:

$$\Delta E = \sqrt{(L^* - L_0)^2 + (a^* - a_0)^2 + (b^* - b_0)^2} \quad (1)$$

where L_0, a_0 and b_0 were the references. L*, a*, and b* values were measured values after the coating preparation process [33, 34] where L_0, a_0 and b_0 corresponded to the target military camouflage reference coating.

2.3.2. CIE 1931 Analysis

Chromaticity analysis of the investigated samples was performed in the CIE 1931 color space [35, 36]. The x and y chromaticity coordinates were determined from the color measurement data, and the correlated color temperature (CCT) values were calculated accordingly. The resulting coordinates were represented on the CIE 1931 chromaticity diagram, and the corresponding chromaticity and CCT values were reported in tabular form.

3. Results and Discussion

In this study, the surface color properties of hybrid epoxy coatings reinforced with graphene, boron carbide, zinc borate, and organic fibres were systematically investigated using the color space (L*, a*, b*) and total color difference (ΔE*ab, CIE 1976) parameters. The experimental program was designed and optimized using the Box–Behnken design. In the experimental setup established based on four factors and three

levels, L* values ranged from 17.09 to 71.55. The highest L* value (71.55) was obtained for the graphene-free formulation containing 1% zinc borate, while significant surface darkening was observed with increasing graphene content. The a* values ranged from -2.18 to +0.27, and most samples were located in the greenish-gray region, with negative a* values The b* values were positive, ranging from 0.65 to 2.96, indicating that the coatings generally exhibited a warm-toned color character. ΔE (color difference) values obtained from the Box–Behnken experimental design quantitatively reflected the effect of different additive components on the surface color. ΔE represented the total color difference between the reference sample and the coating measured during color analysis. Therefore, low ΔE values indicated high color homogeneity and optical stability, whereas high ΔE values indicated significant color deviations. According to color difference perception thresholds defined in CIE-based studies, ΔE values below critical limits corresponded to visually uniform and optically stable surfaces, whereas higher ΔE values indicated perceptible tonal deviations [37].

ΔE values ranged from 2.39 to 47.13. The lowest color difference was obtained for the composition containing 0.5% graphene, 0% boron carbide, 1% zinc borate, and 1% organic fiber (No. 16). This result showed that the combined use of graphene and organic fiber increased surface optical stability and provided a more homogeneous color distribution. In samples with high combined ratios of boron carbide and zinc borate, the ΔE values exceeded 20, resulting in visually noticeable tonal differences in surface color. The general trend showed that increasing the graphene ratio reduced the ΔE value relative to the reference military camouflage coating, thereby suppressing color differences and producing a more neutral surface appearance. In contrast, high levels of zinc borate and

boron carbide increased white-to-gray tonal transitions, resulting in a significant increase in the ΔE value. These results showed that nano additive components played a direct role in adjusting the surface color and that the optical stability of the composite system was highly sensitive to formulation composition. ΔE values were calculated and optimized using black color parameters as a reference. In evaluating the color stability and spectral visibility performance of the developed coating, the study of Michalski et al. [29] on military camouflage coatings was chosen as a reference. The factors were coded as follows: A: Graphene, B: Boron Carbide, C: Zinc Borate, D: Organic Fiber (Table 1). Graphene content (A) emerged as the most influential parameter ($F = 127.80$, $p < 0.0001$). Changes in graphene content caused significant differences in the ΔE value, indicating that graphene played a major role in surface color homogeneity. This behavior was attributed to the strong light-absorbing nature of graphene, which reduced surface reflectivity and suppressed color differences in polymer-based coating systems [38].

The second most influential factor was boron carbide (B) ($F = 7.53$, $p = 0.0158$). This additive led to significant changes in color difference, especially combined with graphene.

The AB interaction term showed that graphene and boron carbide together produced a synergistic balance in surface optics. The main effects of organic fiber (D) and zinc borate (C) were found to be weaker ($p = 0.0521$ and $p = 0.6159$, respectively). The graphene (A) coefficient was relatively high and negative (–11.46). This indicated that increasing the amount of graphene significantly reduced the ΔE value, thereby minimizing the color difference and resulting in a more homogeneous surface appearance. Graphene's dark, light-absorbing nature reduced surface reflectivity, suppressing color differences relative to the reference. The white, reflective nature of zinc

borate reduced color contrast.

Table 1. Box-Behnken design experimental setup for color parameters.

No	A	B	C	D	L*	a*	b*	ΔE
1	1	0.5	1	1	25.23	-2.00	1.13	2.61
2	0.5	0.5	1	0.5	27.33	-1.75	1.01	3.62
3	1	0.5	0	0.5	26.85	-1.65	0.86	3.14
4	0	1	1	0.5	47.10	-0.92	2.72	22.85
5	0.5	0.5	0	0	28.20	-1.67	0.81	4.25
6	0.5	1	0	0.5	26.76	-1.76	0.98	3.18
7	0.5	1	1	1	26.43	-1.82	1.10	3.05
8	0.5	0	0	0.5	34.82	-1.03	0.72	10.45
9	0	0.5	2	0.5	46.10	-0.91	2.42	21.82
10	0	0	1	0.5	71.55	0.27	1.89	47.13
11	0.5	0	1	0	38.90	-1.83	0.65	14.57
12	0.5	0.5	2	0	27.18	-2.18	0.82	3.67
13	0.5	0.5	1	0.5	26.01	-1.78	1.01	2.73
14	0.5	1	2	0.5	27.54	-1.60	1.01	3.72
15	1	0.5	2	0.5	26.65	-1.80	1.05	3.16
16	0.5	0	1	1	26.18	-1.01	0.95	2.39
17	0.5	0.5	1	0.5	26.71	-1.80	0.98	3.17
18	1	1	1	0.5	38.03	-1.31	0.79	13.66
19	0.5	1	1	0	27.10	-1.64	0.98	3.38
20	0.5	0	2	0.5	28.03	-1.73	0.79	4.12
21	0	0.5	0	0.5	49.54	-0.65	2.49	25.23
22	0.5	0.5	1	0.5	26.39	-1.82	0.94	2.95
23	1	0	1	0.5	28.48	-1.69	0.98	4.55
24	0	0.5	1	0	58.08	-1.22	2.38	33.74
25	0.5	0.5	0	1	20.92	-1.71	1.02	4.19
26	0	0.5	1	1	41.44	-0.45	2.96	17.29
27	0.5	0.5	2	1	17.09	-1.70	1.04	7.71
28	0.5	0.5	1	0.5	26.94	-1.85	1.03	3.38
29	1	0.5	1	0	27.19	-1.67	0.96	3.45
30	0	0	0	0	87.64	-2.00	1.13	2.61
Ref	-	-	-	-	24.48	-0.02	-0.40	0.00

The second-order model for the ΔE response was given in Eq. 2 as follows:

***Final Equation in Terms of Coded Factors*:**

$$\Delta E = +3.17 - 11.46A - 2.78B - 0.52C - 2.15D + 8.35AB + 0.86AC + 3.90AD + 1.72BC + 2.96BD + 1.02CD + 12.27A^2 + 4.08B^2 - 0.73C^2 - 0.019D^2$$

(2)

Determining ΔE values in the CIE L*a*b* color space and comparing them with thresholds in the NO-80-A200 military standard provided a reliable framework for optimizing parameters critical in aviation applications, such as surface stability, and long-term color consistency. Therefore, black color parameters were used as a reference when optimizing ΔE limits in color difference analyses in this study. The results of the analysis of variance (ANOVA) performed for the ΔE response showed that the model was highly significant. ($F = 18.70$, $p < 0.0001$) (Table 2).

Table 2. ANOVA analysis

Response: ΔE	**Sum of Squares**	**df**	**Mean Square**	**F-Value**	**p-Value**
Model	3227.52	14	230.54	18.70	< 0.0001
A-Graphene (w/w) (%)	1575.29	1	1575.29	127.80	< 0.0001
B-Boron Carbide (w/w) (%)	92.80	1	92.80	7.53	0.0158
C-Zinc Borate (w/w) (%)	3.24	1	3.24	0.26	0.6159
D-Organic Fiber (w/w) (%)	55.56	1	55.56	4.51	0.0521
AB	278.72	1	278.72	22.61	0.0003
AC	2.94	1	2.94	0.24	0.6328
AD	60.92	1	60.92	4.94	0.0432
BC	11.80	1	11.80	0.96	0.3445
BD	35.11	1	35.11	2.85	0.1136
CD	4.20	1	4.20	0.34	0.5686
A^2	976.96	1	976.96	79.26	< 0.0001
B^2	107.71	1	107.71	8.74	0.0104
C^2	3.42	1	3.42	0.28	0.6065
D^2	2.280E-003	1	2.280E-003	1.850E-004	0.9893
Lack of Fit	172.07	10	17.21	140.87	0.0001
Residual	172.56	14	12.33		
Cor Total	3400.08	28			
Lack of Fit Tests					
Linear	1672.70	20	83.64	684.69	< 0.0001

Response: ΔE	Sum of Squares	df	Mean Square	F-Value	p-Value
2FI	1279.01	14	91.36	747.92	< 0.0001
Quadratic*	172.07	10	17.21	140.87	0.0001
Cubic	77.02	2	38.51	315.26	< 0.0001
Pure Error	0.49	4	0.12		
*Suggested					

The model statistics demonstrated the adequacy of the Box–Behnken models developed for the L*, a*, b*, and ΔE responses in Table 3. The L*, a*, and b* models showed strong agreement with high R^2 (0.99), adjusted R^2, and predicted R^2 values, indicating that color coordinates could be modelled with high accuracy based on additive composition. The R^2 value for the ΔE model was 0.9492, and the lower adjusted and predicted R^2 values were attributed to the fact that ΔE was a more complex response involving the combined effects of multiple color coordinates. However, Adequate Precision values well above 4 for all responses confirmed that the signal to noise ratio was sufficient and that the models had reliable predictive capacity. Low coefficients of variation (C.V. < 7%) for L*, a*, and b* indicated high reproducibility of the experimental data, whereas the higher C.V. value for ΔE suggested greater variability in this response. This value indicated that the total color difference inherently exhibited a wider distribution. Considering the PRESS values as well, the developed models were concluded to be statistically sufficient for estimating and optimizing color coordinates and ΔE within the examined design space.

Table 3. Statistical summary and goodness of fit parameters of the developed response surface models.

Model Parameters	L*	a*	b*	ΔE
Standard Deviation	1.50	0.071	0.083	3.51

Model Parameters	L*	a*	b*	ΔE
Mean	32.72	−1.47	1.26	9.63
C.V. %	4.60	4.82	6.57	36.47
R-Squared	0.9920	0.9912	0.9922	0.9492
Adjusted R-Squared	0.9840	0.9824	0.9844	0.8985
Predicted R-Squared	0.9550	0.9524	0.9567	0.7083
PRESS	177.97	0.38	0.53	991.91
Adequate Precision	48.245	46.288	36.849	16.767

The ΔE prediction performance of the response surface model developed using the Box–Behnken experimental design was demonstrated. The predicted values showed good agreement with the experimental ΔE results around the 45° line, indicating that the model operated with high accuracy throughout the studied range. The distribution of internally studentized residuals versus the predicted values was random, with all points remaining within the ±3 limits. This result indicated that the model did not exhibit systematic errors, outliers, or heteroscedasticity. Consequently, the developed model was confirmed to be statistically adequate and reliable for ΔE estimation and optimization The correlation between the predicted and experimental values was also found to be quantitatively high ($R^2 = 0.9492$). This value showed that the model could explain approximately 95% of the variability in color difference within the studied dataset (Figure 1).

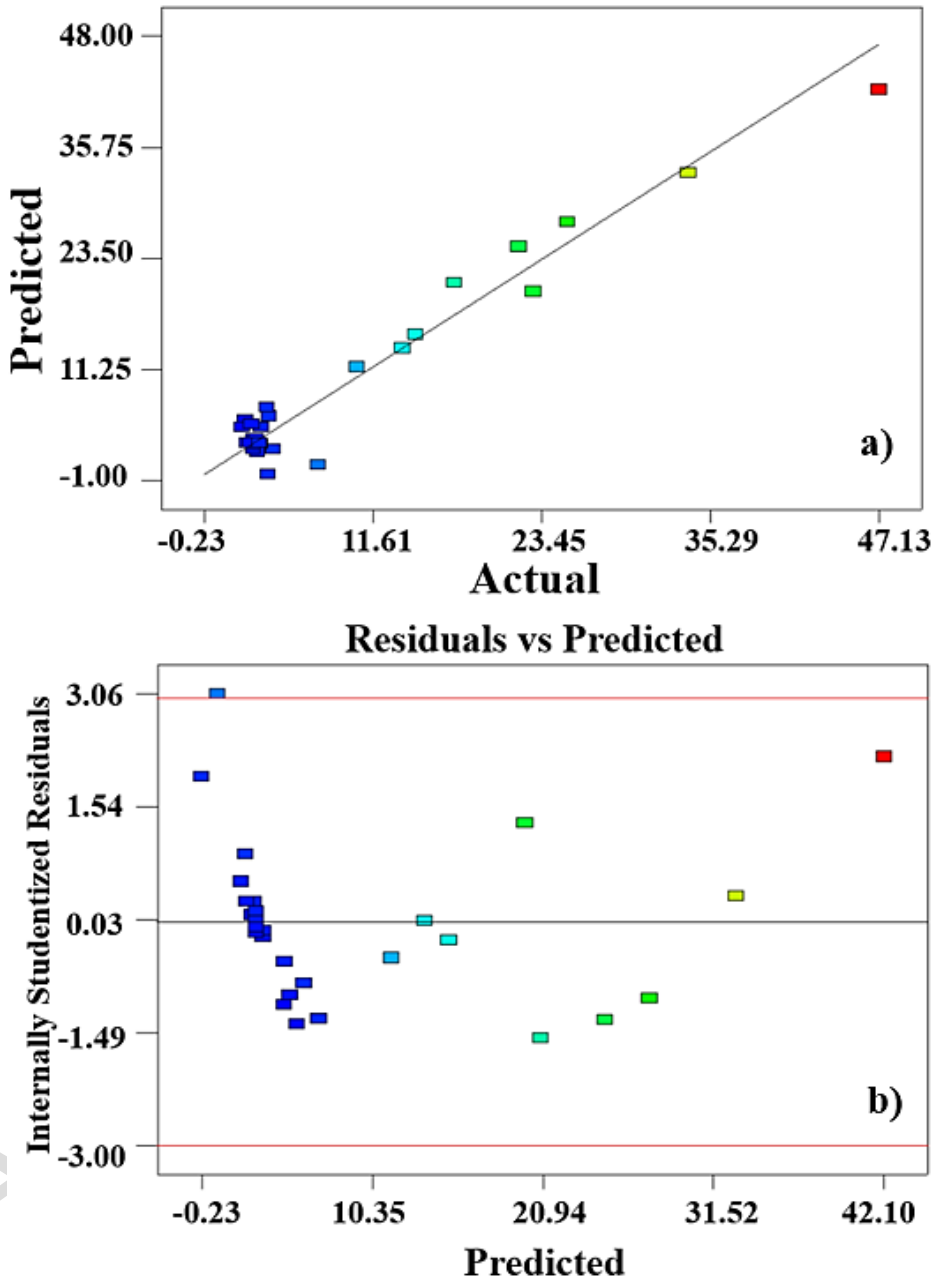

Figure 1. Diagnostic plots for the ΔE response: (a) predicted versus actual values and (b) residuals versus predicted values.

The curves in Figure 2 showed the effect of each additive (A: graphene, B: boron carbide, C: zinc borate, D: organic fiber) on ΔE. Graphene (A) was the component with the most significant effect. The curve was distinctly parabolic, with a rapid decrease in ΔE followed by a slight increase as the graphene content increased from level -1 to level +1.

This reflected the bidirectional effect of graphene, which minimized the color difference at moderate levels but increased it again when used in excessive amounts. Boron carbide (B) also contributed to the reduction of ΔE. The effects of zinc borate (C) and organic fiber (D) on ΔE were quite limited, and the corresponding curves were nearly horizontal.

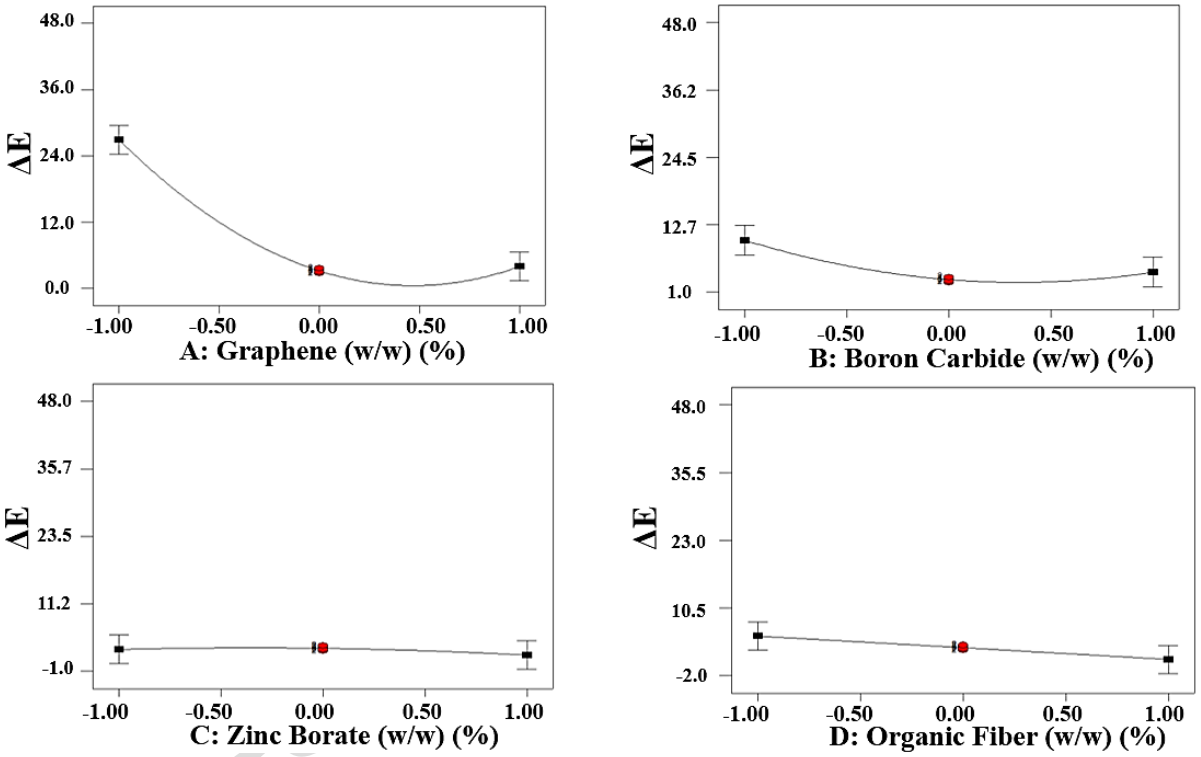

Figure 2. Main effects and single factor interaction plots illustrating the influence of individual variables on the ΔE response.

Figure 3 demonstrated that the ΔE response was mainly governed by the graphene content and its combined behavior with the other formulation variables. The strongest changes in ΔE were observed in plots involving factor A, particularly in the A–B, A–C, and A–D combinations, confirming the dominant role of graphene in the color difference response. By contrast, the B–C, B–D, and especially C–D combinations showed relatively smaller variations, suggesting weaker interaction behavior between these factors. Overall, the plots indicate that ΔE could be reduced within specific intermediate

factor ranges, supporting the suitability of the statistical model for optimization of coating color properties.

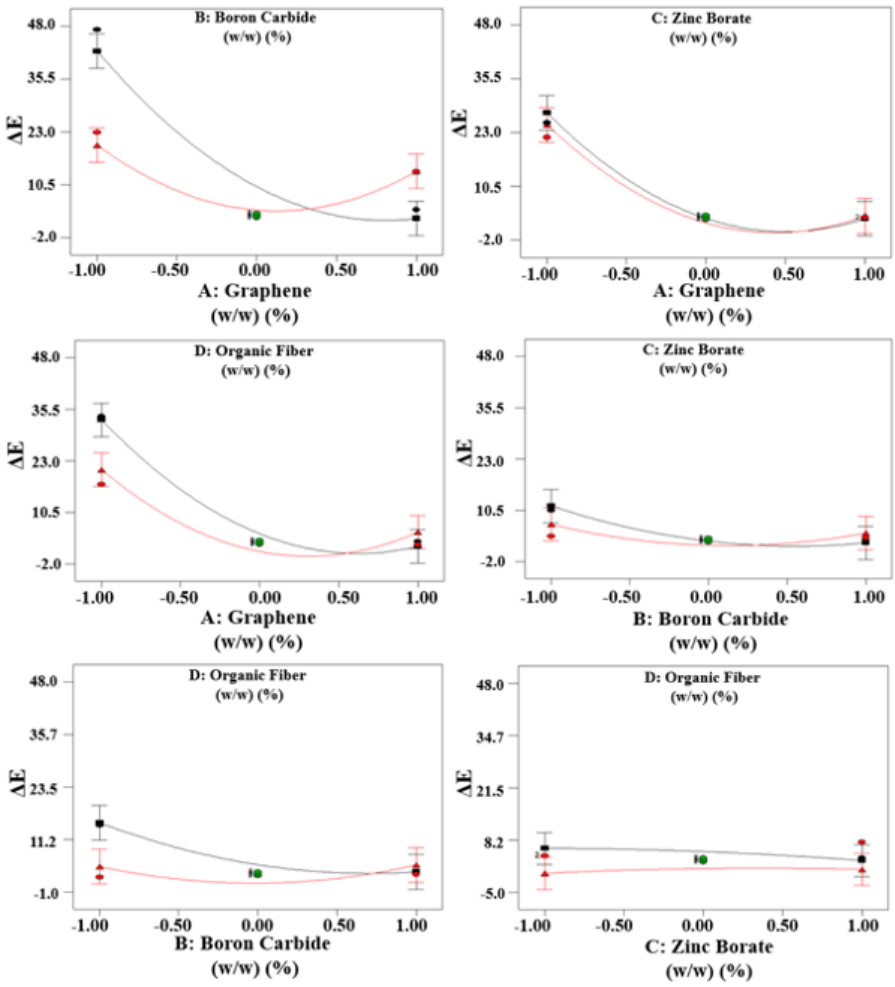

Figure 3. Factor effect plots showing the influence of formulation variables on the ΔE response

Figure 4a showed that factor A (graphene) had the strongest effect on the ΔE response, as indicated by the steepest deviation from the reference point. Factor B (boron carbide) also influenced ΔE, although to a lesser extent than A, whereas factors C (zinc borate) and D (organic fiber) exhibited comparatively smaller effects within the studied range. In Figure 4b, the residuals were distributed approximately along a straight line, indicating that the

normality assumption was reasonably satisfied and that the developed quadratic model was statistically acceptable for representing the ΔE response.

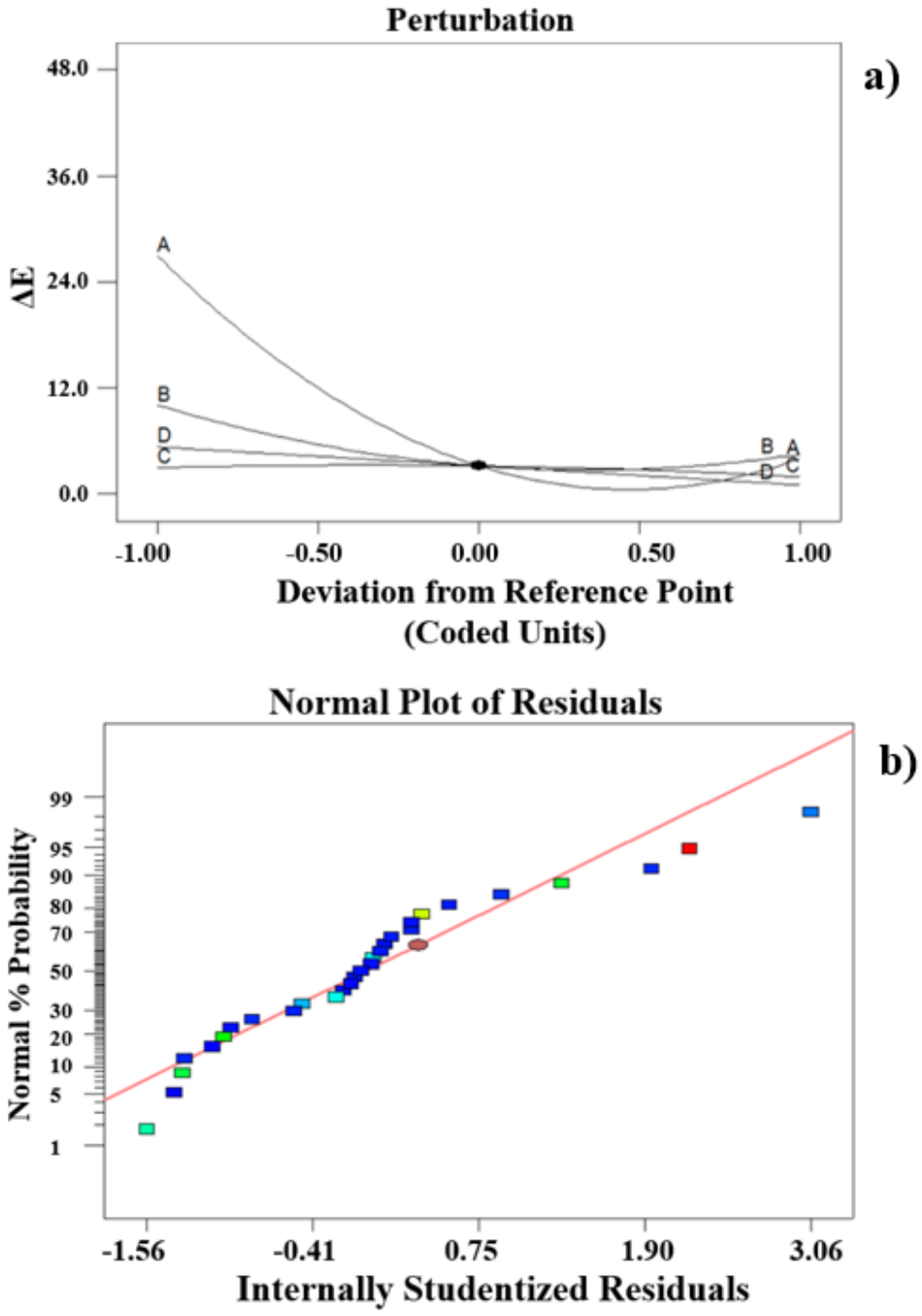

Figure 4. Diagnostic plots for the developed ΔE model: (a) perturbation plot showing the relative influence of formulation variables on the colour difference response, and (b) normal probability plot of residuals used to assess the normality assumption of the model errors

The 3D surface plots in Figure 5 illustrated the combined effect of each factor pair on ΔE. A simultaneous increase in graphene and boron carbide led to a significant decrease in ΔE. ΔE was high in regions with low graphene content, and the color difference decreased rapidly as the graphene content increased. Graphene and boron carbide showed a synergistic effect at certain ratios, but excessive boron carbide addition disrupted this synergy. Increasing the amount of graphene reduced ΔE, while the zinc borate had a weaker effect. Fiber addition appeared to balance the microstructural differences created by boron carbide, thereby reducing the color difference.

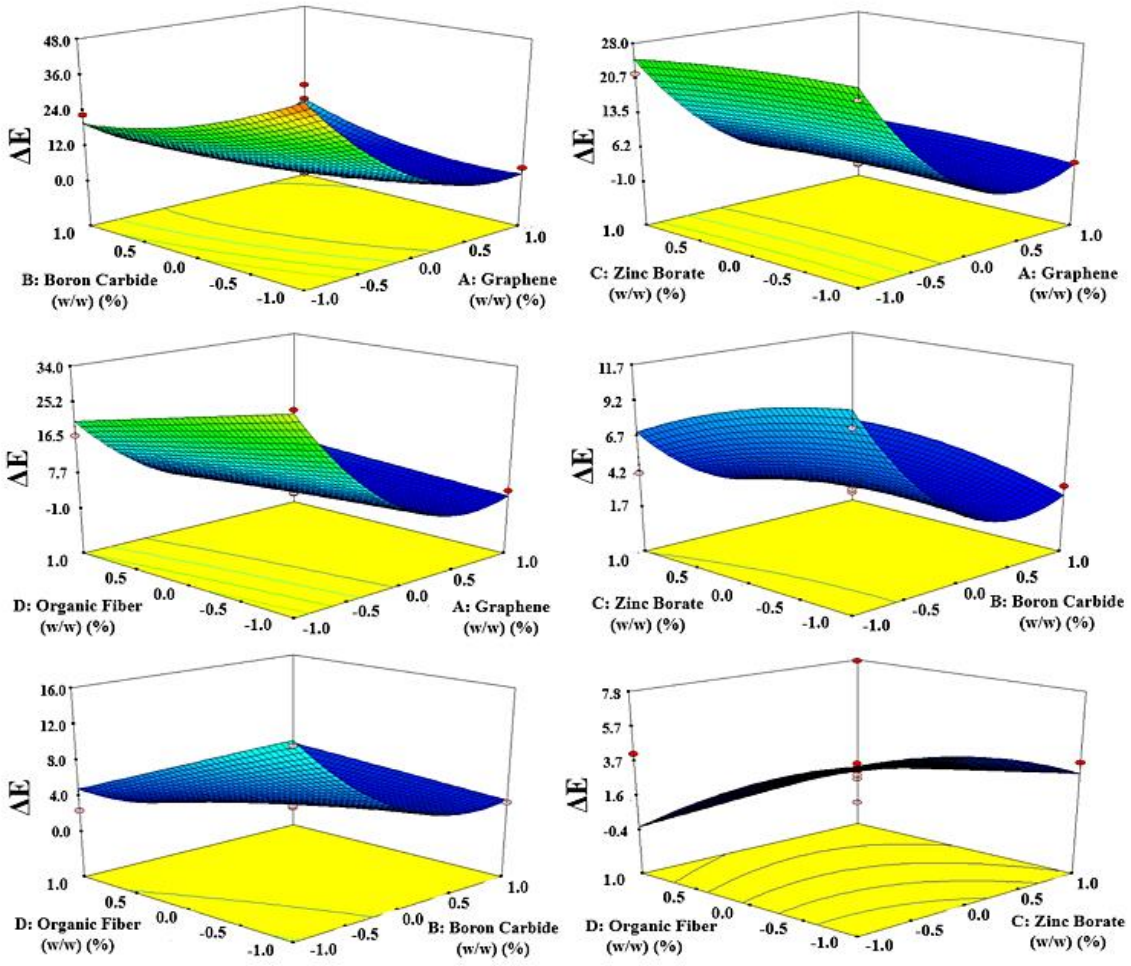

Figure 5. 3D response surface plots illustrating the combined effects of process variables on the ΔE response.

Figure 6 presented a microstructural comparison of coating surfaces optimized for L*, a*, b*, and ΔE using optical microscope images obtained at 100× magnification. The surface optimized for L* (Figure 6a) showed a more homogeneous texture and fewer surface defects. On the surface corresponding to a* optimization (Figure 6b), linear tracks and oriented micro-scratches were more prominent. In the coating optimized for b* (Figure 6c), microcrack-like structures and heterogeneous surface distributions were attributed to the irregular distribution of pigment and filler phases associated with the yellow–blue axis of the b* coordinate. In contrast, the surface optimized for ΔE (Figure 6d) showed a more stable microstructure, a more uniform distribution of phases, and fewer surface defects. These findings demonstrated that ΔE optimization could improve microstructural integrity by promoting a more homogeneous distribution of additive components on the surface. Previous studies have shown that improved filler dispersion and microstructural homogeneity contributed to enhanced optical stability and long-term color retention in epoxy coatings [39, 40].

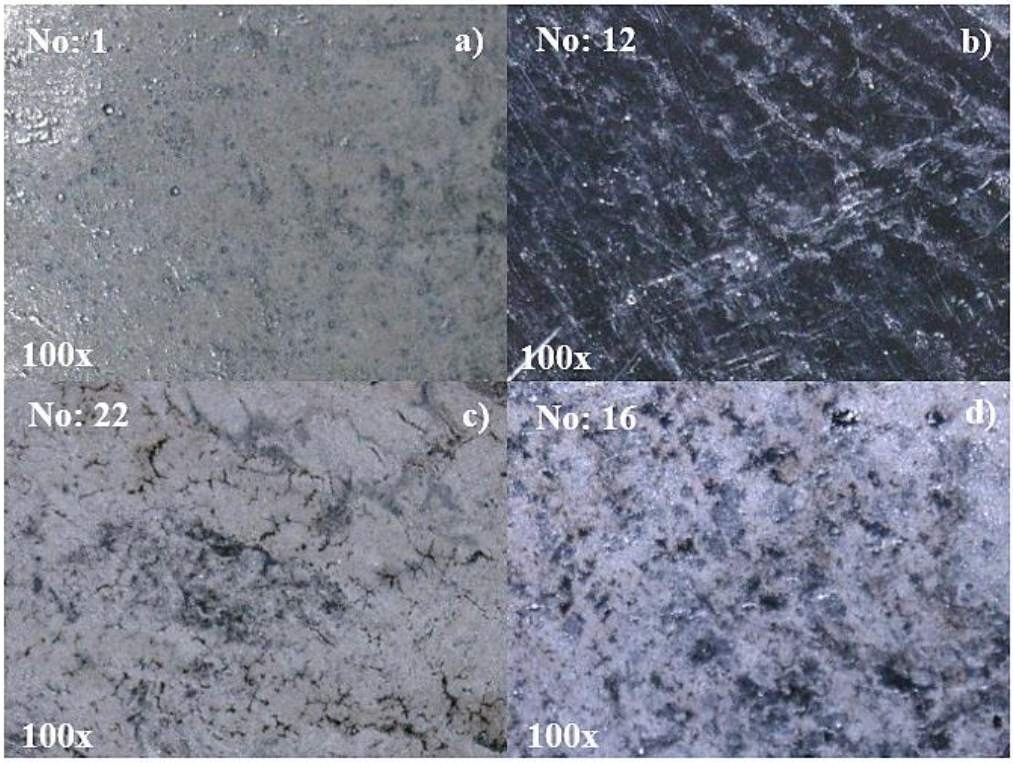

Figure 6. Optical microscope images (100× magnification) showing the surface morphology of the coatings at the optimized conditions based on (a) L*, (b) a*, (c) b* and (d) ΔE.

The chromaticity coordinates of the investigated samples were determined in the CIE 1931 color space and were presented in Figure 7, while the corresponding values are summarized in Table 4. The calculated coordinates were found to be concentrated within a narrow region of the chromaticity diagram, with x values ranging approximately between 0.31 and 0.32 and y values between 0.33 and 0.34.

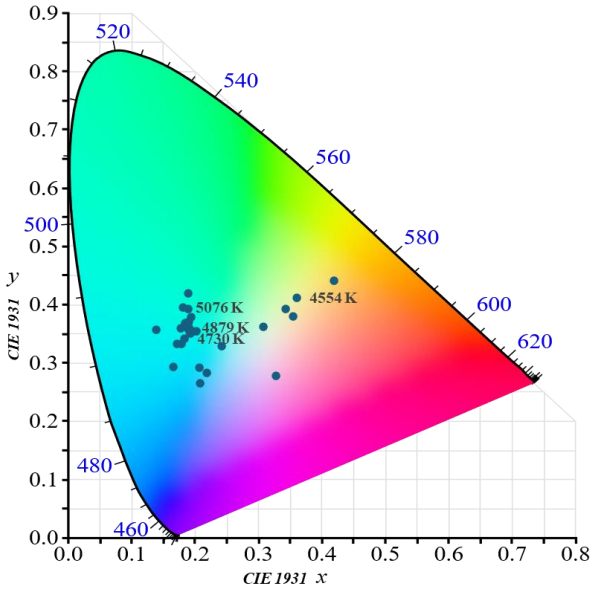

Figure 7. CIE 1931 chromaticity diagram showing the chromaticity coordinates (x, y) of the samples together with their corresponding correlated color temperature (CCT) values.

Based on these chromaticity coordinates, the correlated color temperature (CCT) values were calculated, yielding results predominantly within the range of approximately 4550–5076 K. This temperature interval corresponded to the neutral to daylight white region of the chromaticity diagram. The clustering of the samples within this limited region indicated that only minor variations in chromaticity occurred among the investigated specimens. Furthermore, the reference sample exhibited chromaticity coordinates of approximately x = 0.31 and y = 0.33 with a correlated color temperature of about 4571 K, which was consistent with the chromaticity region occupied by the other samples. Overall, the results demonstrated that the investigated samples exhibit similar chromatic characteristics.

Table 4. CIE 1931 chromaticity coordinates (x, y) and correlated color temperature (CCT) values calculated for the investigated samples

No	x	y	CCT (K)
1	0.31	0.34	4637
2	0.31	0.34	4646
3	0.31	0.34	4628
4	0.32	0.34	4964
5	0.31	0.34	4617
6	0.31	0.34	4638
7	0.31	0.34	4654
8	0.31	0.33	4677
9	0.32	0.34	4927
10	0.32	0.33	4879
11	0.31	0.33	4584
12	0.31	0.34	4554
13	0.31	0.34	4641
14	0.31	0.34	4665
15	0.31	0.34	4647
16	0.31	0.34	4730
17	0.31	0.34	4633
18	0.31	0.33	4659
19	0.31	0.34	4653
20	0.31	0.34	4605
21	0.32	0.34	4947
22	0.31	0.34	4622
23	0.31	0.34	4648
24	0.32	0.34	4857
25	0.31	0.34	4650
26	0.32	0.34	5076
27	0.31	0.34	4655
28	0.31	0.34	4637
29	0.31	0.34	4646
30	0.31	0.33	4654
Ref	0.31	0.33	4571

Table 5 presented a comparison of the coating formulations determined to be optimum, namely No. 1 (L*), No. 12 (a*), No. 22 (b*), and No. 16 (ΔE), with respect to additional performance parameters such as coating thickness, contact angle, tensile strength, displacement [41], and

gloss. No significant differences or performance losses were observed among the optimum formulations in terms of coating thickness and mechanical properties. All optimum conditions were found to preserve structural integrity. The contact angle and mechanical parameter values showed that optical optimization did not adversely affect the functional properties of the coatings. These results showed that ΔE-based optimization could provide a balanced combination of visual compatibility and other fundamental coating performance properties.

Table 5. Auxiliary surface, mechanical and optical properties measured for the formulations optimized with respect to L*, a*, b* and ΔE

Parameters	**L***	**a***	**b***	**ΔE**
Thickness of coating (µm)	125.78	197.48	191.01	183.66
Contact angle (°)	66.44	81.47	85.80	72.66
Tensile strength (MPa)	130.57	140.37	131.91	145.99
Displacement (mm)	18.53	12.67	15.50	16.01
Gloss (GU)	41.70	32.50	54.60	99.70

The coatings were stored for approximately six months under ambient laboratory light exposure, followed by storage under uncontrolled ambient conditions, reaching a total storage period of approximately one year. The color stability of the ΔE-optimized coating was further evaluated after approximately one year of ambient storage, including six months of exposure to ambient laboratory light. Since no standardized aging or weathering protocol was applied, this assessment was treated as an exploratory storage stability check rather than a durability test. Color coordinates (L*, a*, b*) were re-measured using the same instrument and measurement protocol as the initial measurements. The calculated ΔEstore value, representing the color difference between the initial and stored states, remained below unity, indicating minimal color drift over the

storage period. These results suggested that the ΔE-based optimisation provided an initial color match to the target camouflage reference and maintained acceptable color stability under prolonged ambient storage and light exposure conditions. Although the applied storage conditions did not represent controlled aging, the low ΔEstore value indicated that the color matching achieved through ΔE minimization was not limited to the initial state and remained stable over time under non-aggressive environmental conditions (Table 6).

Table 6. ΔE-based color stability of the ΔE-optimized coating after one year of ambient storage, including six months of ambient light exposure

Parameters	**Optimum**	**After storage**
L*	26.18	25.45
a*	-1.01	-1.48
b*	0.95	1.25
ΔE	**0.92**	

4. Conclusion

The main conclusions of this study are as follows:

1. The color performance of hybrid water-based epoxy coatings containing graphene, boron carbide, zinc borate, and peanut shell-derived organic fiber was successfully assessed using CIE L*a*b parameters and ΔE-based optimization.
2. The Box–Behnken design and response surface methodology yielded statistically reliable models for predicting the color responses. The developed models showed high accuracy, with R^2 values of 0.9920, 0.9912, 0.9922, and 0.9492 for L*, a*, b*, and ΔE, respectively.

3. Graphene was the most influential factor affecting color difference, while boron carbide showed a secondary effect. ANOVA confirmed that the ΔE response was mainly governed by the main effect of graphene together with its interaction and quadratic terms.
4. The optimum formulation for ΔE minimization was obtained at 0.5% graphene, 0% boron carbide, 1% zinc borate, and 1% organic fiber, giving the lowest ΔE value of 2.39, which indicated the closest match to the target military camouflage reference coating.
5. CIE 1931 chromaticity analysis showed that all coatings were concentrated within a narrow chromaticity region $(x \approx 0.31–0.32,\ y \approx 0.33–0.34)$, with correlated color temperature values ranging from 4554 to 5076 K, indicating similar chromatic characteristics among the investigated samples.
6. The ΔE-optimized coating maintained acceptable auxiliary properties and storage stability. No major deterioration was observed in the additional performance parameters, and the ΔE_{store} value remained below 1 after approximately one year of ambient storage, indicating only minor color drift over time.

5. References

1. Shunmugapriya K, Kale SS, Gouda G, Jayapal P, Tamilmani K. Paints for aerospace applications. In: Prasad NE, Wanhill RJH, editors. Aerospace Materials and Material Technologies. Springer; p. 539-562, 2017. https://doi.org/10.1007/978-981-10-2143-5

2. Peltier F, Thierry D. Review of CR-free coatings for the corrosion protection of aluminum aerospace alloys. Coatings. 2022; 12(4): 518. https://doi.org/10.3390/coatings12040518

3. Hegedus CR, Spadafora SJ, Eng AT. Aerospace and aircraft coatings. In: Koleske JV, editor. Paint and Coating Testing Manual: 15th Edition of the Gardner-Sward Handbook. ASTM International; 2012. p. 739–750. https://doi.org/10.1520/MNL12239M

4. Visser P, Terryn H, Mol JMC. Aerospace coatings. In: Visser P, Terryn H, Mol JMC, editors. Active Protective Coatings. Springer; 2016. p. 315–372. https://doi.org/10.1007/978-94-017-7540-3_12

5. Wang S, Wang D, An Q, Li J, Chong K, Wang X, et al. Multi-regional natural aging behaviors and degradation mechanisms of polyurethane-coated fabrics under coupled multiple environmental factors. Polymers. 2025; 17(19): 2634. https://doi.org/10.3390/polym17192634

6. Yang X, Vang C, Tallman D, Bierwagen G, Croll S, Rohlik S. Weathering degradation of a polyurethane coating. Polym Degrad Stab. 2001; 74(2): 341–351. https://doi.org/10.1016/S0141-3910(01)00166-5

7. Ranjbar Z, Montazeri S, Jalili M. Optimization of a waterborne epoxy coatings formulation using experimental design. Prog Color Color Coat. 2009; 2(1): 23–33. https://doi.org/10.30509/pccc.2009.75748

8. Samyn P, Bosmans J, Cosemans P. Benchmark study of epoxy coatings with selection of bio-based phenalkamine versus fossil-based amine crosslinkers. Molecules. 2023; 28(11): 4259. https://doi.org/10.3390/molecules28114259

9. Xu H, Yaguchi H, Shioiri S. Testing CIELAB-based color-difference formulae using large color differences. Opt Rev. 2001; 8(6): 487–494. https://doi.org/10.1007/BF02931740
10. Usmani AM, Donley M. Aircraft-coating weathering studies by analytical methods. J Appl Polym Sci. 2002; 86(2): 294-313. https://doi.org/10.1002/app.10960
11. Zhang T, Zhang T, He Y, Wang Y, Bi Y. Corrosion and aging of organic aviation coatings: A review. Chin J Aeronaut. 2023; 36(4): 1–35. https://doi.org/10.1016/j.cja.2022.12.003
12. Taylor S, Sieradzki K. The development of a multi-functional aerospace coating: Considerations in the use of nano-dimensioned materials. Prog Org Coat. 2003; 47(3): 169-173. https://doi.org/10.1016/S0300-9440(03)00136-X
13. Hu J, Li X, Gao J, Zhao Q. UV aging characterization of epoxy varnish coated steel upon exposure to artificial weathering environment. Mater Des. 2009; 30(5): 1542–1547. https://doi.org/10.1016/j.matdes.2008.07.051
14. Sung L, Stanley D, Gorham JM, Rabb S, Gu X, Yu LL, et al. A quantitative study of nanoparticle release from nanocoatings exposed to UV radiation. J Coat Technol Res. 2015; 12(1): 121-135. https://doi.org/10.1007/s11998-014-9620-9
15. Baig MMA, Samad MA. Epoxy/epoxy composite/epoxy hybrid composite coatings for tribological applications—A review. Polymers. 2021; 13(2): 179. https://doi.org/10.3390/polym13020179
16. Da Silva MS, De Souza AG, Rosa DDS, Valera TS, Wiebeck H. Greener waterborne epoxy coatings with optimized UV-resistance. Polímeros. 2024; 34(3): e20240034. https://doi.org/10.1590/0104-1428.20230133

17. Schulte S, Schäfer H, Vogel C, Shah V, Kroll S, Siebert-Raths A. Environmentally resistant flax fiber-reinforced composites for aircraft applications. Appl Compos Mater. 2025; 32: 1975–1995. https://doi.org/10.1007/s10443-024-10296-z
18. Sanko V, Aydemir Sezer Ü, Basağaoğlu Demirekin Z, Eroğlu E, Türkaslan S, Sezer S. Investigation of the mechanical and color properties of microcrystalline cellulose-containing dental composite resins. Atatürk Univ Fac Dent J. 2020; 30(2): 181–187. https://doi.org/10.17567/ataunidfd.652319
19. Yan X, Han Y, Yin T. Coating process optimization and self-healing performance evaluation of shellac microcapsules coated with melamine/rice husk powder. Appl Sci. 2021; 11(18): 8373. https://doi.org/10.3390/app11188373
20. Virág ÁD, Suplicz A, Török D. Prediction of the thermal degradation-induced color change of acrylonitrile butadiene styrene products as a function of temperature and titanium dioxide content. Results Eng. 2024; 24: 103505. https://doi.org/10.1016/j.rineng.2024.103505
21. Andrés-Herguedas L, Pozo-Antonio JS, Alonso-Villar EM. Protection of contemporary mural artwork: Evaluation of a fixing primer and color protectors. Prog Org Coat. 2025; 204: 109252. https://doi.org/10.1016/j.porgcoat.2025.109252
22. Chee SS, Jawaid M, Sultan MTH, Alothman OY, Abdullah LC. Accelerated weathering and soil burial effects on color, biodegradability and thermal properties of bamboo/kenaf/epoxy hybrid composites. Polym Test. 2019; 79: 106054. https://doi.org/10.1016/j.polymertesting.2019.106054

23. Ma J, Ruan S, Hu J, Sun Y, Fei Y, Jiang X, et al. The intrinsic relationship between color variation and performances of the deteriorated aviation lubrication oil. J Ind Eng Chem. 2020; 92: 88–95. https://doi.org/10.1016/j.jiec.2020.08.023

24. LeVesque RJ II, Jones CA, Babel HW. Clear, colored and black anodic coatings for passive thermal control of the International Space Station. In: 25th International Conference on Environmental Systems (ICES); 1995 Jul 10; San Diego, CA. SAE Technical Paper 951653. https://doi.org/10.4271/951653

25. Asadipour H, Alizadeh M, Ashrafizadeh F. Evaluation of graphene transparent coating on copper for color and oxidation control at low temperatures. Diamond Relat Mater. 2022; 130: 109502. https://doi.org/10.1016/j.diamond.2022.109502

26. Aliyeva M, Şahin Fİ, Acaralı N. Comprehensive analysis on design expert modelling for solvent-free coating with halloysite/Malaysian rice/tobacco/linseed oil hybrid system as green inhibitors in maritime applications. J Adhes Sci Technol. 2025: 1-17. https://doi.org/10.1080/01694243.2025.2570852

27. Bay ZM, Şahin Fİ, Acaralı N. Development of green coatings with mineral modifiers and natural fillers. Period. Mineral. 2025; 94: 135-146. https://doi.org/10.13133/2239-1002/18898

28. Öztürk N, Şahin Fİ, Acaralı N. Enhancing surface properties with coconut oil/cocoa butter/chia seed/titanium dioxide: Innovations in water-based coating technologies. J Am Oil Chem Soc. 2024; 102(3): 533-545. https://doi.org/10.1002/aocs.12903

29. Michalski M, Pisarek U. The influence of operational exposure on changes in parameters of effective camouflage of coatings used in military technology. Adv Sci Technol Res J. 2023; 17(1): 182-196. https://doi.org/10.12913/22998624/156940

30. Suzuki T, Ito C, Kitano K, Yamaguchi T. CIELAB color space as a field for tracking color-changing chemical reactions of polymeric pH indicators. ACS Omega. 2024; 9(34): 36682-36689. https://doi.org/10.1021/acsomega.4c05320
31. Chow WS, Yap YP. Optimization of process variables on flexural properties of epoxy/organo-montmorillonite nanocomposite by response surface methodology. eXPRESS Polym Lett. 2008; 2(1): 2-11. https://doi.org/10.3144/expresspolymlett.2008.2
32. Ahmadi S, Mohammadi L, Igwegbe CA, et al. Application of response surface methodology in the degradation of Reactive Blue 19 using H_2O_2/MgO nanoparticles advanced oxidation process. Int J Ind Chem. 2018; 9: 241–253. https://doi.org/10.1007/s40090-018-0153-4
33. Kubheka P, Shange S, Deenadayalu N, Mdluli P, Mokhothu T. Exploration of CIELAB color system for the colorimetric detection of lead ions in environmental water using gold nanoparticles. Results Chem. 2025; 18: 102785. https://doi.org/10.1016/j.rechem.2025.102785
34. Winhard J, Nestler D, Kroll L. Effects of process parameters in thermoforming of unidirectional fibre-reinforced thermoplastics. Polymers. 2024; 16(2): 221. https://doi.org/10.3390/polym16020221
35. Ohno Y. CIE fundamentals for color measurements. In: NIP & Digital Fabrication Conference. 2000. p. 540-545. https://doi.org/10.2352/ISSN.2169-4451.2000.16.1.art00033_2

36. Kim J, Oh H, Kim A, Kim J, Lee E, Baek J, et al. A study on detection of glucose concentration using changes in color coordinates. Bioengineered. 2016; 8(1): 99-104. https://doi.org/10.1080/21655979.2016.1227629

37. Sharma G, Wu W, Dalal EN. The CIEDE2000 color-difference formula: Implementation notes, supplementary test data, and mathematical observations. Color Res Appl. 2004; 30(1): 21-30. https://doi.org/10.1002/col.20070

38. Zhu Y, Murali S, Cai W, Li X, Suk JW, Potts JR, et al. Graphene and graphene oxide: Synthesis, properties, and applications. Adv Mater. 2010; 22(35): 3906-3924. https://doi.org/10.1002/adma.201001068

39. Christopher G, Kulandainathan MA, Harichandran G. Biopolymers nanocomposite for material protection: Enhancement of corrosion protection using waterborne polyurethane nanocomposite coatings. Prog Org Coat. 2016; 99: 91-102. https://doi.org/10.1016/j.porgcoat.2016.05.012

40. Bierwagen GP. Reflections on corrosion control by organic coatings. Prog Org Coat. 1996; 28(1): 43-48. https://doi.org/10.1016/0300-9440(95)00588-9

41. Şahin Fİ, Okumuş Y, Acaralı N. Displacement behavior in nano-modified epoxy coatings: A Box-Behnken approach. J Indian Chem Soc. 2026; 103(3): 102452. https://doi.org/10.1016/j.jics.2026.102452